

**Exploratory study on the masses of odd- Z nuclei and r -process
simulation based on the deformed relativistic Hartree-Bogoliubov
theory in continuum**

C. Pan (潘琮)

Department of Physics, Anhui Normal University, Wuhu 241000, China

Y. C. Yang (杨曜尘) and X. F. Jiang (姜晓飞)

*State Key Laboratory of Nuclear Physics and Technology,
School of Physics, Peking University, Beijing 100871, China*

X. H. Wu (吴鑫辉)*

Department of Physics, Fuzhou University, Fuzhou 350108, Fujian, China

(Dated: March 13, 2025)

Abstract

Background: Nuclear masses of exotic nuclei are important for both nuclear physics and astrophysics. The deformed relativistic Hartree-Bogoliubov theory in continuum (DRHBc) is capable of providing proper descriptions for exotic nuclei by simultaneously including deformation and continuum effects. The mass table of even- Z nuclei with $8 \leq Z \leq 120$ has been established based on the DRHBc theory[At. Data Nucl. Data Tables 158, 101661 (2024)].

Purpose: This work aims to systematically estimate the masses of odd- Z nuclei based on the available DRHBc results of even- Z nuclei, thereby providing a pseudo DRHBc mass table for all nuclei with $8 \leq Z \leq 120$. This mass table can then be employed in the r -process studies to investigate the influence of deformation on r -process.

Method: The mass of an odd nucleus is expressed as a function of the masses and odd-even mass differences of its neighboring even nuclei, with the odd-even mass difference approximated by the average pairing gap. The r -process simulations are carried out using the site-independent classical r -process model based on the waiting-point approximation.

Results and Conclusions: The approximation of the odd-even mass difference with the average pairing gap is validated to be effective, by reproducing the masses of even- Z odd- N nuclei calculated by DRHBc. Combining the DRHBc masses of even- Z nuclei and the estimated masses of odd- Z , a pseudo DRHBc mass table is established, with the root-mean-square (rms) deviation from available mass data $\sigma = 1.50$ MeV. This pseudo DRHBc mass table is applied to the r -process simulation, and the impact of nuclear deformation effects is analyzed. The deformation effects can influence the r -process path and thus affect the r -process abundance. In particular, the nuclear shape transitions can even lead to the discontinuity of the r -process path.

* Contact author: wuxinhui@fzu.edu.cn

I. INTRODUCTION

Nuclear masses are important for both nuclear physics [1] and astrophysics [2]. They reflect a variety of underlying physical effects of nuclear quantum many-body systems, and can be used to extract nuclear structure information, e.g., nuclear deformation [3], shell effects [4], and nuclear force [5]. They also determine the reaction energies for all nuclear reactions, which are important in understanding the energy production in stars [6] and the study of nucleosynthesis [7]. Experimentally, the masses of about 2500 nuclei have been measured so far [8].

The rapid neutron capture process (r -process) has been believed to be responsible for the nucleosynthesis of about half of the elements heavier than iron for more than half a century [9–11]. The understanding of r -process is still affected by the uncertainties in our knowledge of both nuclear physics quantities and astrophysical conditions [2, 11–14]. The masses of neutron-rich nuclei are crucial to the r -process studies, as they are needed to extract the reaction energies that go into the calculations of all involved nuclear reaction rates, i.e., neutron separation energies (S_n) for neutron-capture cross sections and β -decay Q -values (Q_β) for β -decay half-lives ($T_{1/2}$) [15, 16]. Even in the classical r -process model with waiting-point approximation (WPA), the use of different nuclear mass models would affect the equilibrium between neutron capture and photodisintegration reactions to predict r -process path and also the Q -values of β -decay half-lives, and thus affect the final calculated abundance [17]. Nuclear masses of most neutron-rich nuclei, especially the exotic nuclei near drip lines, remain beyond the current experimental capabilities even in the foreseeable future, due to the difficulties in production, separation, and detection. Therefore, theoretical models with reliable predictive power are essential.

Many efforts have been made to theoretically describe nuclear masses, including macroscopic-microscopic models [18–21], microscopic models [22–27], and machine-learning approaches [28–38]. Microscopic models are usually believed to have a better reliability of extrapolation [39–41]. This is particularly necessary for the mass predictions for the exotic nuclei, which are far away from the experimentally known region and play important roles in the r -process path.

The exotic nuclei involved in the r -process path are extremely weakly bound, and their Fermi energies are very close to the continuum threshold. For these nuclei, the pairing

interaction can scatter nucleons from bound states to the resonant ones in the continuum, and the density could become more diffuse due to this coupling to the continuum [42]. The stability of exotic nuclei and even the position of the drip line might be influenced, which is the so-called continuum effect. Therefore, the effects of pairing correlation and the coupling to continuum should be considered properly [43–48] in the description for exotic nuclei near drip lines. This is important for the studies of r -process in extremely high-neutron-density environments, e.g., the neutron star mergers. The relativistic continuum Hartree-Bogoliubov (RCHB) theory [49, 50] takes into account pairing correlations and continuum effect in a microscopic and self-consistent way, and has achieved great success in describing both stable and exotic nuclei [42, 51]. Based on the RCHB theory, the first nuclear mass table including continuum effect was constructed [25], and the continuum effect on the limits of the nuclear landscape was studied. However, the accuracy of the RCHB mass table is limited due to the assumed spherical symmetry.

Most nuclei in the nuclear chart, except for doubly magic ones, exhibit deformed shapes. In order to properly describe deformed exotic nuclei, the deformed relativistic Hartree-Bogoliubov theory in continuum (DRHBc) was developed by treating the effects of deformation, pairing correlations, and continuum simultaneously [52, 53]. As the advantages of the RCHB theory are inherited and the deformation degree of freedom is further included, the DRHBc theory has been successfully applied in a variety of studies on exotic nuclei, including the halo structures [54–65], peninsulas beyond the neutron drip line [40, 41, 66, 67], evolution of deformation and shape coexistence [68–71], half-life estimation for proton emission and α -decay [72–74], etc. The predictive power of the DRHBc theory for nuclear mass has been examined in Refs. [40, 41] by taking the even-even superheavy nuclei with $102 \leq Z \leq 120$ as examples. Recently, based on the DRHBc theory, a nuclear mass table for the nuclei with $8 \leq Z \leq 120$ is in progress [75, 76]. The DRHBc mass table is expected to provide the first microscopic mass input with the effects of deformation and continuum simultaneously included. Up to now, the even- Z part of the DRHBc mass table has been established [27, 77].

Since the results for odd- Z nuclei are unavailable in the DRHBc mass table, our work aims to systematically estimate their masses based on the available results of even- Z nuclei, and then utilize them to perform r -process simulations. This article is structured as follows: The theoretical frameworks for the DRHBc theory and classical r -process are briefly introduced

in Section II, the masses of odd- Z nuclei are estimated in Section III, the r -process simulation based on the obtained masses is discussed in Section IV, and finally, a summary is given in Section V.

II. THEORETICAL FRAMEWORK

A. The DRHBc theory

The details of the DRHBc theory have been illustrated in Refs. [53, 75, 76]. In this Section, we just present a brief theoretical framework. In the DRHBc theory, the motion of nucleons are microscopically described by the relativistic Hartree-Bogoliubov (RHB) equation [78],

$$\begin{pmatrix} \hat{h}_D - \lambda_\tau & \hat{\Delta} \\ -\hat{\Delta}^* & -\hat{h}_D^* + \lambda_\tau \end{pmatrix} \begin{pmatrix} U_k \\ V_k \end{pmatrix} = E_k \begin{pmatrix} U_k \\ V_k \end{pmatrix}, \quad (1)$$

where \hat{h}_D is the Dirac Hamiltonian, $\hat{\Delta}$ is the pairing potential, E_k is the quasiparticle energy, U_k and V_k are the quasiparticle wave functions, and λ_τ is the Fermi energy of neutron or proton ($\tau = n, p$).

In the coordinate space, the Dirac Hamiltonian \hat{h}_D reads

$$h_D(\mathbf{r}) = \boldsymbol{\alpha} \cdot \mathbf{p} + V(\mathbf{r}) + \beta[M + S(\mathbf{r})], \quad (2)$$

where $S(\mathbf{r})$ and $V(\mathbf{r})$ are scalar and vector potentials, respectively. The pairing potential $\hat{\Delta}$ reads

$$\Delta(\mathbf{r}_1, \mathbf{r}_2) = V^{pp}(\mathbf{r}_1, \mathbf{r}_2)\kappa(\mathbf{r}_1, \mathbf{r}_2), \quad (3)$$

where V^{pp} is the pairing force, and κ is the pairing tensor [79]. In this work, the density-dependent zero-range pairing force

$$V^{pp}(\mathbf{r}_1, \mathbf{r}_2) = V_0 \frac{1}{2} (1 - P^\sigma) \delta(\mathbf{r}_1 - \mathbf{r}_2) \left(1 - \frac{\rho(\mathbf{r}_1)}{\rho_{\text{sat}}} \right) \quad (4)$$

is adopted.

In the DRHBc theory, the axial deformation and spatial reflection symmetry are assumed, and the potentials and densities can be expanded in terms of the Legendre polynomials,

$$f(\mathbf{r}) = \sum_{\lambda} f_{\lambda}(r) P_{\lambda}(\cos \theta), \quad \lambda = 0, 2, 4, \dots, \lambda_{\text{max}}. \quad (5)$$

For the exotic nuclei close to drip lines, the continuum effect should be taken into account properly [42, 44]. For this purpose, the deformed RHB equations (1) are solved in a spherical Dirac Woods-Saxon basis [80, 81], which can properly describe the asymptotic behavior of the density distribution at a large r for exotic nuclei.

For a nucleus with odd number of neutron or proton, the blocking effect of the unpaired nucleon(s) needs to be considered [79]. Practically, this can be realized by the exchange of quasiparticle wavefunctions $(U_{k_b}, V_{k_b}) \leftrightarrow (V_{k_b}^*, U_{k_b}^*)$ and that of the energy $E_{k_b} \leftrightarrow -E_{k_b}$ for Eq. (1), where k_b refers to the blocked orbital for the odd nucleon [76, 82].

After self-consistently solving the RHB equations, the expectation values such as binding energy, quadrupole deformation, root-mean-square radii, etc., can be calculated [53, 75, 76]. The canonical basis $|\psi_i\rangle$ is obtained by the following diagonalization [79]:

$$\hat{\rho} |\psi_i\rangle = v_i^2 |\psi_i\rangle, \quad (6)$$

where $\hat{\rho}$ is the density matrix, and v_i^2 is the corresponding occupation probability of $|\psi_i\rangle$. The single-particle energy in the canonical basis is obtained as $\epsilon_i = \langle \psi_i | \hat{h}_D | \psi_i \rangle$. The pairing gap Δ_i is calculated by

$$\Delta_i = \frac{2u_i v_i}{u_i^2 - v_i^2} (\epsilon_i - \lambda_\tau), \quad (7)$$

where the parameter u_i is obtained from $u_i^2 + v_i^2 = 1$. The average pairing gap defined by [44, 83]:

$$\Delta = \frac{\sum_i v_i^2 \Delta_i}{\sum_i v_i^2}, \quad (8)$$

is an order parameter describing the phase transition from a normal fluid to a superfluid [84].

B. Classical r -process

In this work, a site-independent r -process model, i.e., the so-called classical r -process model, is employed to specifically study the effect of nuclear mass on the r -process simulation. Classical r -process model can be regarded as a realistic simplification of the dynamical r -process model, and has been successfully employed in describing r -process patterns of both the solar system and metal-poor stars [85–88]. Nevertheless, it should be noted that the real neutron freeze-out after the equilibrium between neutron capture and photodisintegration

reactions, as well as the fission recycling, are neglected in the present classical r -process model.

In the classical r -process model, iron group seed nuclei are irradiated by high-density neutron sources with a high temperature $T \gtrsim 1.5$ GK. The r -process abundances are obtained by the superposition of abundances from the simulations in 16 different neutron flows with neutron densities in the range of $10^{20} - 10^{27.5}$ cm^{-3} . The weight ω and the irradiation time τ of each neutron flow follow exponential relations on neutron density n_n [85, 89]:

$$\begin{aligned}\tau(n_n) &= a \times n_n^b, \\ \omega(n_n) &= c \times n_n^d.\end{aligned}\tag{9}$$

The parameters a , b , c , and d can be determined from a least-square fit to the solar r -process abundances.

In the astrophysical environments with high-temperature $T \gtrsim 1.5$ GK and high neutron density $n_n \gtrsim 10^{20}$ cm^{-3} , the equilibrium between neutron capture and photodisintegration reactions can be achieved, and the abundance ratios of neighboring isotopes on an isotopic chain can be obtained by the Saha equation [90–92]

$$\frac{Y(Z, A+1)}{Y(Z, A)} = n_n \left(\frac{2\pi\hbar^2}{m_\mu kT} \right)^{3/2} \frac{G(Z, A+1)}{2G(Z, A)} \left(\frac{A+1}{A} \right)^{3/2} \times \exp \left[\frac{S_n(Z, A+1)}{kT} \right], \tag{10}$$

where $Y(Z, A)$, $S_n(Z, A)$, and $G(Z, A)$ are, respectively, the abundance, one-neutron separation energy, and partition function of nuclide (Z, A) , and \hbar , k , and m_μ are the Planck constant, Boltzmann constant, and atomic mass unit, respectively. Note that the neutron separation energy S_n deduced from nuclear masses appears in the exponential, suggesting the importance of nuclear masses in the equilibrium.

The abundance flow from one isotopic chain to the next is governed by β decays and can be expressed by a set of differential equations

$$\frac{dY(Z)}{dt} = Y(Z-1) \sum_A P(Z-1, A) \lambda_\beta^{Z-1, A} - Y(Z) \sum_A P(Z, A) \lambda_\beta^{Z, A}, \tag{11}$$

where $\lambda_\beta^{Z, A}$ is the β decay rate of the nucleus (Z, A) , $Y(Z) = \sum_A Y(Z, A) = \sum_A P(Z, A)Y(Z)$ is the total abundance of each isotopic chain. By using Eqs. (10) and (11), the abundance of each isotope can be determined. After the neutrons freeze-out, the unstable isotopes on the neutron-rich side will proceed to the stable isotopes mainly via β decays, and the final abundances are obtained.

III. PSEUDO DRHBC MASS TABLE

The even-even and even- Z odd- N parts of the DRHBC mass table have been completed, with the numerical details and results summarized in Refs. [27, 77], respectively. Since the odd- Z part of the DRHBC mass table is not yet available, a proper estimation for the masses of odd- Z nuclei would provide preliminary insights into the knowledge of the whole nuclear landscape and the applications in the r -process simulation.

A. Mass estimation for odd nuclei

The mass of an odd nucleus can be estimated by the interpolation based on the properties of its neighboring even nuclei [93, 94]. Here we first give a brief introduction of the estimation, and then perform examinations by taking all even- Z odd- N nuclei in the nuclear chart with $8 \leq Z \leq 120$ as examples.

The binding energy E_b of a nucleus can be expressed in terms of the combinations of its neighbors' quantities, for example,

$$E_B(Z, N) = \frac{1}{2}[E_b(Z, N+1) + E_b(Z, N-1)] - \frac{1}{2}[\delta_n(Z, N+1) + \delta_n(Z, N-1)], \quad (12)$$

$$\text{or } E_B(Z, N) = \frac{1}{2}[E_b(Z+1, N) + E_b(Z-1, N)] - \frac{1}{2}[\delta_p(Z+1, N) + \delta_p(Z-1, N)], \quad (13)$$

where δ_n and δ_p are the three-point odd-even mass differences for neutron and proton, respectively, defined as

$$\delta_n(Z, N) = \frac{(-1)^N}{2}[2E_b(Z, N) - E_b(Z, N+1) - E_b(Z, N-1)], \quad (14)$$

$$\delta_p(Z, N) = \frac{(-1)^Z}{2}[2E_b(Z, N) - E_b(Z+1, N) - E_b(Z-1, N)]. \quad (15)$$

The odd-even mass difference is often approximated by the average pairing gap in Eq. (8) [43, 95–97],

$$\delta_n(Z, N) \approx \Delta_n(Z, N), \quad \delta_p(Z, N) \approx \Delta_p(Z, N). \quad (16)$$

With this approximation, the E_b of an odd nucleus can be obtained based on the E_b and $\Delta_{n/p}$ of its neighboring even nuclei, where the latter ones have already been provided in a

self-consistent and microscopic manner from the available part of the DRHBc mass table [27, 77]. Such an interpolation treatment on odd nuclei is simple, but contains the nuclear structure information from microscopic calculations to a certain extent, and thus ensures that the magnitude of pairing correlations is correct [93].

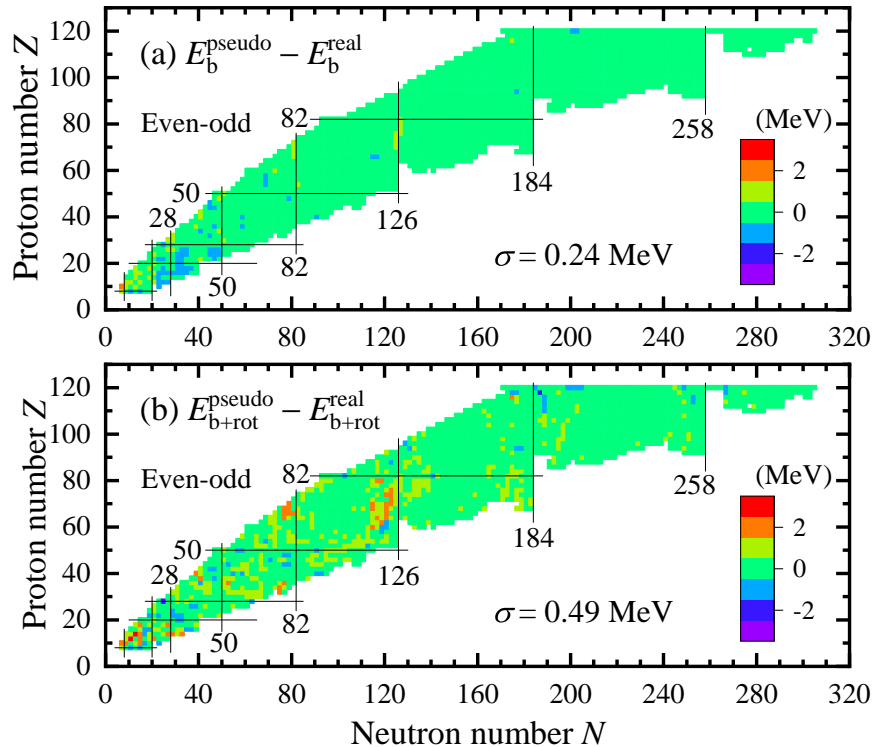


FIG. 1. The differences between the pseudo and real DRHBc results for the binding energies of even-odd nuclei with $8 \leq Z \leq 120$ scaled by colors. (a) The rotational correction is not considered. (b) The rotational correction is included.

To examine this interpolation treatment, taking all even- Z odd- N (even-odd for short) nuclei as examples and employing the above interpolation, the binding energies are obtained. Since these interpolated results are not from real DRHBc calculations, for convenience, they are labeled “pseudo” DRHBc results in this work. Figure 1 shows the differences between the pseudo binding energies and the real DRHBc results from self-consistent blocking calculations (labeled as “real”). In Fig. 1(a), where the rotational correction is not considered, for most nuclei the differences between the pseudo and real DRHBc results are less than 0.5 MeV, with the root-mean-square (rms) difference being 0.24 MeV, showing excellent agreement between these two treatments. In comparison, the rms deviation of real DRHBc binding energies (w/o rotational correction) from experimental data for even- Z nuclei is 2.56

MeV [77]. The difference between the two theoretical treatments is dramatically smaller than the deviation from the data. This indicates that the pseudo DRHBc binding energies can well reproduce the real DRHBc results.

For the density functional PC-PK1 adopted here, the rotational correction has been shown to play an important role in improving the binding energy description for deformed nuclei [75, 76, 98]. Therefore, it is necessary to compare E_b^{pseudo} and E_b^{real} after incorporating the rotational correction energy E_{rot} , and the corresponding results are shown in Fig. 1(b). The differences between these two treatments are still less than 0.5 MeV for most nuclei, while we also noticed that some nuclei exhibit larger differences than those in Fig. 1(a). For example, for the nuclei with $N = 121, 123$, $Z \approx 70$, as well as those with $N = 77, 79$, $Z \approx 67$, their $E_{b+\text{rot}}^{\text{pseudo}} - E_{b+\text{rot}}^{\text{real}}$ are larger than 1.5 MeV. These larger differences mainly correspond to the abrupt changes of nuclear shape, especially those near magic numbers, whose deformations suddenly decrease to (near-)zero. In Refs. [27, 77], it was mentioned that the cranking approximation used in DRHBc to obtain the E_{rot} is not suitable for (near-)spherical nuclei, and therefore, for the nuclei with $|\beta_2| < 0.05$, their E_{rot} are taken as zero in the DRHBc mass table. Considering that the $E_{b+\text{rot}}^{\text{pseudo}}$ for an even-odd nucleus in Fig. 1(b) is interpolated based on the $E_{b+\text{rot}}^{\text{real}}$ of its neighboring even-even nuclei, the pseudo result may significantly deviate from the real result when the β_2 values of neighboring even-even nuclei straddle 0.05. Although some nuclei show larger differences, the rms difference in Fig. 1(b) is 0.49 MeV, which is slightly larger than that without E_{rot} in Fig. 1(a), but still much smaller than the rms deviation of $E_{b+\text{rot}}^{\text{real}}$ from the data, 1.43 MeV. Therefore, after including the rotational correction, the pseudo and real DRHBc binding energies are still in good agreement for most nuclei, and their differences are not expected to substantially influence the discussions on physics.

B. Precision of the pseudo mass table

Based on the DRHBc mass table for even- Z nuclei [77] and using Eqs. (12) and (13) ($\delta_{n/p}$ are approximated by $\Delta_{n/p}$), the binding energies of odd- Z nuclei with $8 \leq Z \leq 120$ are estimated. Combining the pseudo binding energies of odd- Z nuclei and the real DRHBc results of even- Z nuclei available, a pseudo DRHBc mass table is obtained. For convenience, here the corresponding binding energy value is labeled as E_b^{pseudo} , which includes both pseudo

results for odd- Z nuclei and real DRHBc results for even- Z nuclei. 9480 bound nuclei are obtained in total, where 2584 (27.3%) are even-even, 2245 (23.7%) are even-odd, 2513 (26.5%) are odd-even, and 2138 (22.6%) are odd-odd.

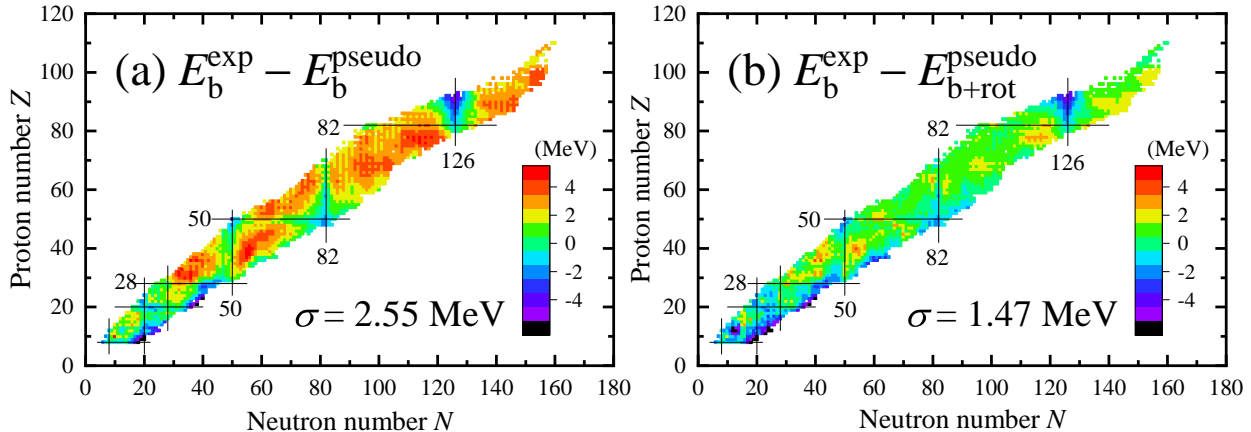


FIG. 2. The differences between the pseudo DRHBc binding energies and the available data [8] for the nuclei with $8 \leq Z \leq 120$ scaled by colors. The details about the pseudo DRHBc results can be found in the text. (a) The rotational correction is not considered. (b) The rotational correction is included.

Among these 9480 bound nuclei, the masses of 2413 nuclei have been measured experimentally [8]. Figure 2 shows the binding energy deviations $E_b^{\text{exp}} - E_b^{\text{pseudo}}$ for these measured nuclei. The results without E_{rot} and with E_{rot} are shown in panels (a) and (b), respectively. In Fig. 2(a), the deviation is relatively small near magic numbers, while it becomes larger when getting far away from magic numbers, which is related to the increase of deformation. The rms deviation of predicted binding energies from data is $\sigma = 2.55$ MeV. In Fig. 2(b), after including the E_{rot} , the binding energy description is significantly improved for most nuclei, especially those with both neutron and proton numbers far away from magic numbers. Accordingly, the rms deviation reduces to $\sigma = 1.47$ MeV. As a comparison, the corresponding rms deviation for real DRHBc binding energies for only even- Z nuclei is $\sigma = 2.56$ MeV without E_{rot} , and $\sigma = 1.43$ MeV with E_{rot} [77]. The rms deviations in Fig. 2 are very close to these two values, respectively, indicating that our pseudo binding energies of odd- Z nuclei reach almost the same accuracy as the real DRHBc results of even- Z nuclei.

The one-neutron separation energy

$$S_n(Z, N) = E_b(Z, N) - E_b(Z, N - 1) \quad (17)$$

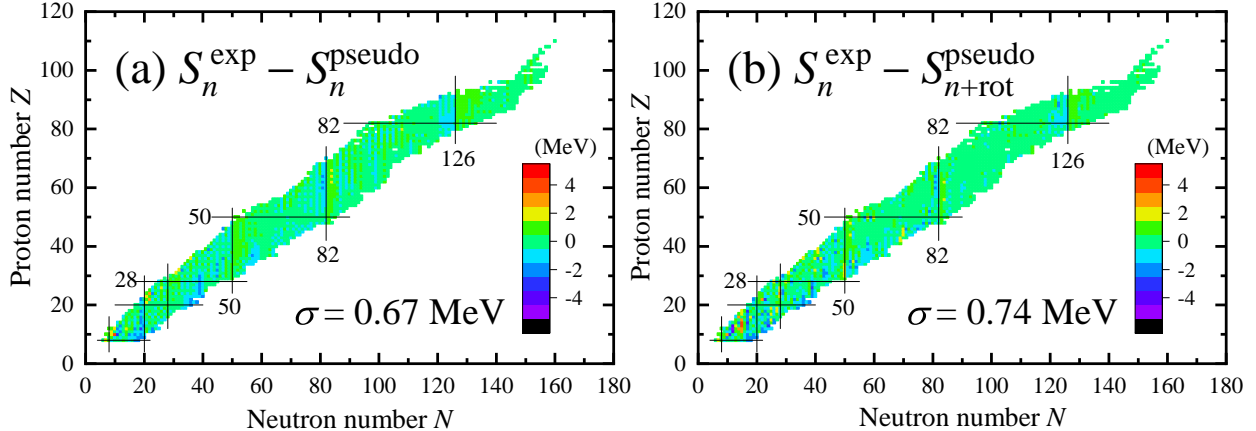


FIG. 3. The differences between the pseudo DRHBc results of one-neutron separation energy and the available data [8] for the nuclei with $8 \leq Z \leq 120$ scaled by colors. (a) The rotational correction is not considered. (b) The rotational correction is included.

is intricately connected to the characteristics of the astrophysical r -process. Utilizing the E_b^{pseudo} in Fig. 2(a), the S_n^{pseudo} without rotational correction is calculated and its deviation from 2299 available data [8] is shown in Fig. 3(a). The deviations for most nuclei are within 1 MeV, and the rms deviation $\sigma = 0.67$ MeV. Figure 3(b) shows the deviation of S_n after including the rotational correction energy. It is found that, generally, E_{rot} improves the description of S_n at $Z > 50$, but for light nuclei the deviation is increased, resulting in the rms deviation $\sigma = 0.74$ MeV, slightly larger than the case without rotational correction in panel (a). The result that E_{rot} does not improve the σ of S_n has been noticed in the calculations on even- Z nuclei [77], and is attributed to the limit of cranking approximation, which has already been discussed in Fig. 1(b). We also noticed that the deviations in some odd- Z nuclei are different from those of their even- Z neighbors, forming odd-even staggering with respect to proton number in Fig. 3. This means that these pseudo results do not fully capture the odd-even effects. We expect that a fully self-consistent treatment in the complete DRHBc mass table in the future would eliminate this staggering in the deviation of S_n .

Similar to the discussions on Figs. 2 and 3, the rms deviations of other predicted quantities, including the two-neutron separation energy S_{2n} and one- and two-proton separation energies S_p, S_{2p} , in the pseudo DRHBc mass table are calculated and summarized in Table I. It is noted that by introducing E_{rot} , the description of E_b is significantly improved, while

TABLE I. The rms deviations σ for binding energies (E_b), one- and two-neutron separation energies (S_n, S_{2n}), as well as one- and two-proton separation energies (S_p, S_{2p}) in the pseudo DRHBc mass table with respect to the available data [8] in the unit of MeV. For comparison, the corresponding deviations for even- Z and odd- Z nuclei are also listed separately.

Range	Theory	$\sigma(E_b)$	$\sigma(S_n)$	$\sigma(S_{2n})$	$\sigma(S_p)$	$\sigma(S_{2p})$
All	Pseudo + real DRHBc (w/o E_{rot})	2.55	0.67	0.93	0.66	0.93
All	Pseudo + real DRHBc (w/ E_{rot})	1.47	0.74	0.96	0.71	0.98
Even- Z	Real DRHBc (w/o E_{rot})	2.56	0.75	0.95	-	0.93
Even- Z	Real DRHBc (w/ E_{rot})	1.43	0.77	0.99	-	1.05
Odd- Z	Pseudo DRHBc (w/o E_{rot})	2.54	0.58	0.89	-	0.93
Odd- Z	Pseudo DRHBc (w/ E_{rot})	1.50	0.70	0.94	-	0.90

for separation energies the corresponding σ values slightly increase, due to the cranking approximation as mentioned in the above discussions. For comparison, the corresponding results for even- Z and odd- Z nuclei are also listed separately in Table I. It is found that odd- Z nuclei have similar σ values to even- Z ones for both binding energies and separation energies, showing the consistency between the pseudo and real DRHBc results.

In conclusion, in this Section, based on the available DRHBc results [77] for even- Z nuclei, the binding energies of odd- Z nuclei are estimated. A complete pseudo DRHBc mass table is obtained for all nuclei with $8 \leq Z \leq 120$, with the accuracies in describing nuclear masses and separation energies expected to be close to the real DRHBc results from self-consistent calculations.

IV. R -PROCESS SIMULATION

The obtained pseudo DRHBc mass table in Section III is applied in the r -process simulation, to study the impact of deformation effects in the r -process. The r -process simulation is performed using the classical r -process model, where nuclear masses are taken from the pseudo DRHBc mass table or the RCHB mass table [25], if the experimental data [8] are not available. For the β -decay rates, the empirical formula [99] using decay energies from the pseudo DRHBc or RCHB calculations is employed together with experimental data [100].

The astrophysical trajectory, i.e., the weight ω and the irradiation time τ of neutron flows, is determined by fitting the obtained abundances to the solar r -process abundances [101] at a temperature of $T = 1.5$ GK.

The r -process abundances with pseudo DRHBc and RCHB mass tables are shown in Fig. 4. It is found that the simulated abundances with both the RCHB and pseudo DRHBc mass tables exhibit abundance peaks near $A = 130, 195$ and an abundance trough around $A = 170$. The r -process abundances based on pseudo DRHBc mass table are higher for $A = 148 - 165$ and lower for $A = 170 - 178$ compared to those based on the RCHB mass table. This indicates the impact from the deformation effects.

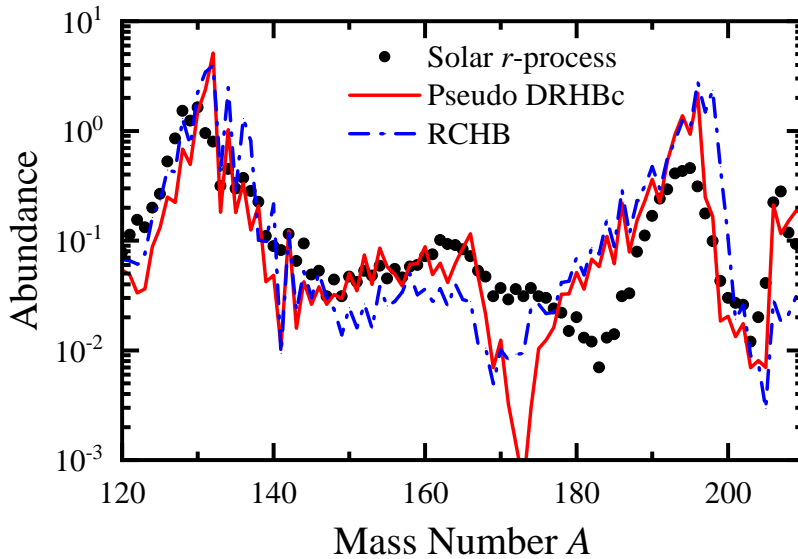


FIG. 4. The r -process abundances from classical r -process simulations based on pseudo DRHBc and RCHB mass tables as functions of the mass number A . The solar r -process abundances [101] are displayed with black dots.

The most important nuclei for the r -process are located in the r -process path. The r -process paths for nuclei with $A \sim 130 - 195$ based on the pseudo DRHBc and RCHB mass tables are displayed in Fig. 5. It is found that the r -process path nuclei around $A = 160$ predicted by the pseudo DRHBc mass table are closer to the stability line than the ones predicted by the RCHB mass table. Since the beta decay half-lives are generally shorter when the nuclei are moving toward the neutron-rich direction, the decay half-lives of r -process path nuclei around $A = 160$ based on the pseudo DRHBc mass table are longer than those based on the RCHB mass table. This results in more nuclei accumulating on

the path nuclei. It is therefore understandable that the r -process abundances based on the pseudo DRHBc mass table are larger for $A = 148 - 165$ than the ones based on the RCHB mass table. On the other hand, it is noted that the r -process path predicted by the pseudo DRHBc mass table has a gap around $A = 175$, which leads to a deficiency in the simulated abundances in this region.

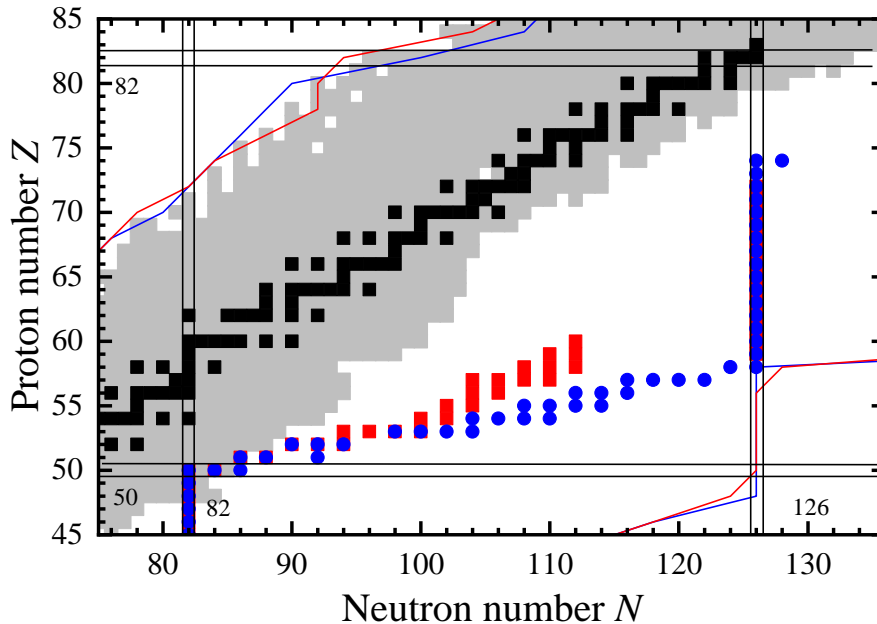


FIG. 5. The r -process path for nuclei with $A \sim 130 - 195$ based on the pseudo DRHBc and RCHB mass tables denoted as red squares and blue squares, respectively. Stable nuclei (black square), experimentally known nuclei [8] (gray square), drip lines predicted by the pseudo DRHBc (red line) and RCHB (blue line) mass tables are also displayed.

Figure 6 shows the differences of nuclear binding energy predicted by the pseudo DRHBc and RCHB mass tables. The differences of nuclear binding energy predictions are relatively small around neutron and proton magic numbers, while they become larger in the middle of the shell. In the simulation, most r -process path nuclei with $A = 134 - 181$ are located in the $N = 82 - 126$ region, where the pseudo DRHBc mass table predicts higher binding energies than the RCHB mass table due to the deformation effect. This leads to the differences of r -process abundances between these two mass models. The mass differences are mainly caused by the deformation effects. Fig. 7 shows the quadrupole deformation β_2 of even- Z nuclei predicted by the DRHBc theory. The spherical and near-spherical nuclei are often

found around neutron and proton magic numbers as expected, and the well-deformed nuclei often appear in the middle of the shell. Meanwhile the prolate-oblate shape changes can be found around $N = 120$ for $50 \leq Z \leq 82$. Notably, the r -process path with $A = 134 - 181$ passes through the region for $N = 82 - 126$. This indicates that the prediction of r -process path with $A = 134 - 181$ is significantly influenced by the deformation effect.

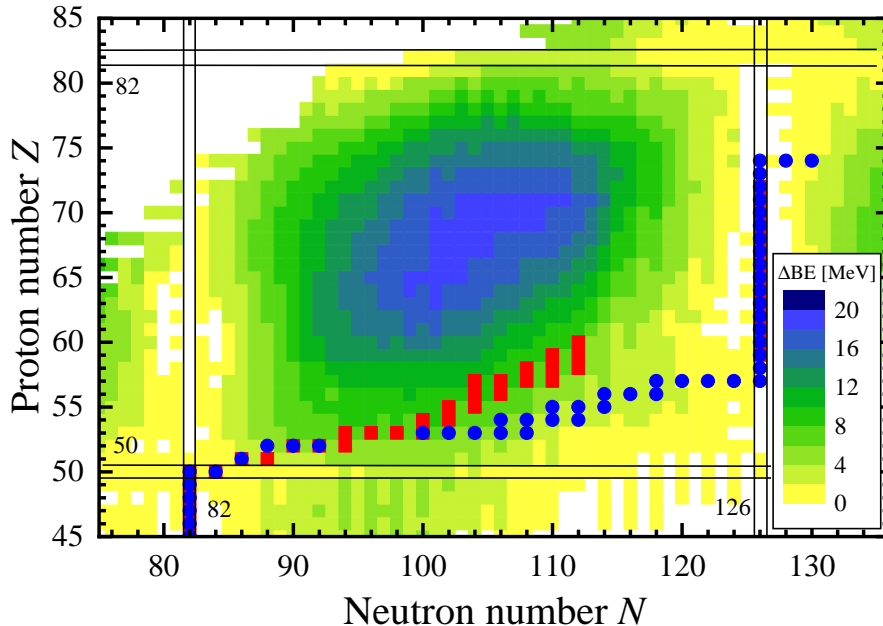


FIG. 6. The binding energy differences for bound nuclei with $82 \leq N \leq 126$ between the pseudo DRHBc calculations and RCHB calculations scaled by colors.

As is evident from Eq. (10), the single neutron separation energy S_n manifests in the exponent, rendering it the primary quantity that has a direct impact on the r -process simulations. Fig. 8 (a) shows the predicted neutron separation energies for the xenon isotopic chain based on the pseudo DRHBc and RCHB mass tables as functions of A . Note that in the present r -process simulations, the neutron flow with neutron number density $n_n = 10^{24.5} \text{ cm}^{-3}$ contributes the most to the abundance near $A = 160$. Therefore, taking the neutron flow with $n_n = 10^{24.5} \text{ cm}^{-3}$ and the xenon ($Z = 54$) isotopic chain as examples, we analyze the impact of the deformation effect on r -process nuclei around $A = 160$. It is found that for the xenon isotopic chain, the neutron separation energies predicted by the pseudo DRHBc mass table decrease more rapidly with A . According to Eq. (10), as shown in Fig 8 (b), the abundance ratios of adjacent even-even nuclei predicted by the pseudo DRHBc mass

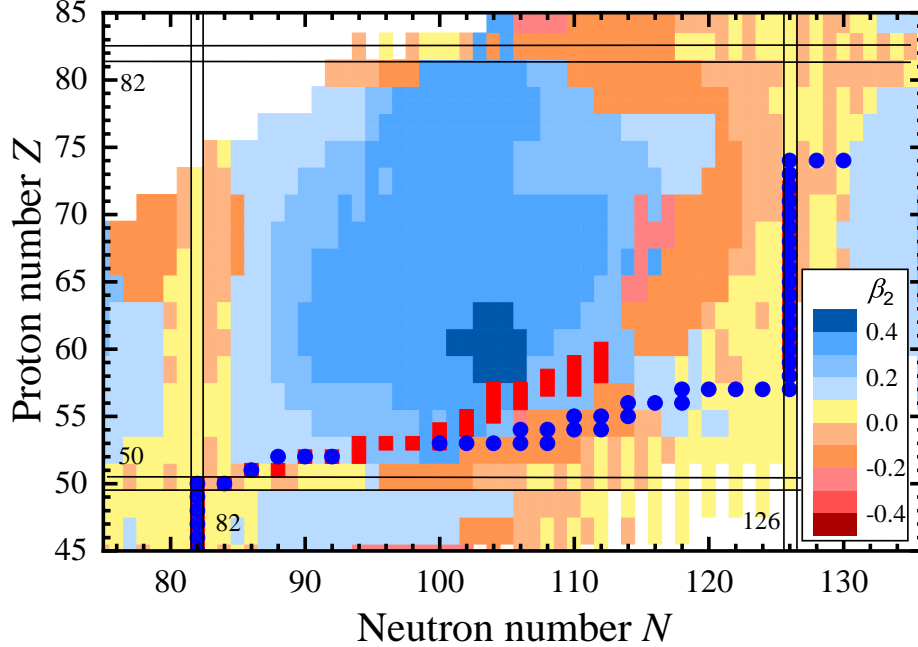


FIG. 7. Quadrupole deformations β_2 from the DRHBc calculations for bound even- Z nuclei with $82 \leq N \leq 126$ scaled by colors.

table decrease more rapidly with A . Additionally, as the mass number A increases, the abundance ratios of adjacent even-even nuclei decrease from several orders of magnitude above 1 to below 1. This indicates that as the neutron number increases, the abundance of even-even nuclei gradually increases until reaching a maximum and then decreases. Fig. 8 (c) shows the relative abundance distribution of even-even nuclei on the xenon isotopic chain. It is found that, compared to the results of the RCHB mass table, the maximum of the abundance distribution, which corresponds to the r -process path nuclei, based on the pseudo DRHBc mass table is located at smaller mass numbers. This is the reason that the r -process abundances based on pseudo DRHBc mass table are higher for $A = 148 - 165$ compared to those based on the RCHB mass table, as shown in Fig. 4.

As for the r -process nuclei around $A = 175$, the neutron flow with neutron number density $n_n = 10^{24} \text{ cm}^{-3}$ and the neodymium ($Z = 60$) isotopic chain are taken to analyze the impact of deformation effect. Figure 9 (b) represents the predicted neutron separation energies for the neodymium isotopic chain based on the pseudo DRHBc and RCHB mass tables as functions of mass number A . It is found that the pseudo DRHBc mass table with rotational corrections predicts a sudden decrease in neutron separation energy at $A = 180$.

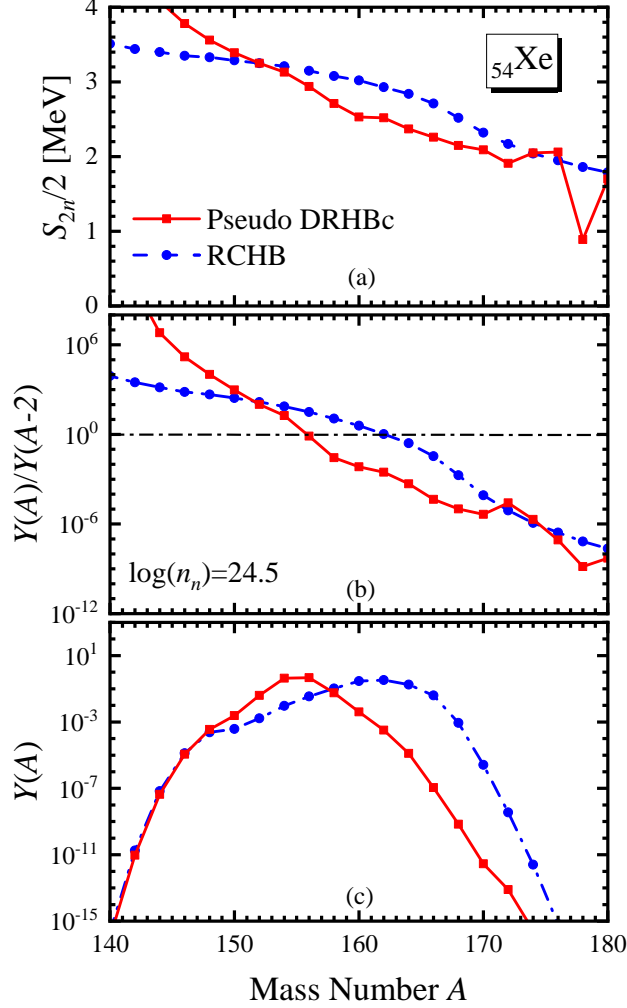


FIG. 8. (a) The neutron separation energies of the xenon isotope chain predicted by the pseudo DRHBc and RCHB mass tables as functions of mass number A . (b) The abundance ratio of adjacent even-even nuclei along the xenon isotope chain predicted by the pseudo DRHBc and RCHB mass tables as functions of mass number A , under astrophysical conditions with neutron number density $n_n = 10^{24.5} \text{ cm}^{-3}$ and temperature $T \gtrsim 1.5 \text{ K}$. (c) Relative abundance distribution of even-even nuclei along the xenon isotope chain predicted by the pseudo DRHBc and RCHB mass tables as functions of mass number A , before the neutrons freeze-out.

This sudden change arises because the DRHBc calculation neglects rotational corrections for nuclei with $|\beta_2| < 0.05$ to avoid numerical challenges [27, 77]. As shown in Fig. 9 (a), the quadrupole deformations β_2 from the DRHBc calculations for neodymium isotopes drop below 0.05 at $A = 180$, causing the sudden reduction in neutron separation energy for this isotope. Consequently, this sharp decline reduces the relative abundance distribution

at $A = 180$. Following the neutron freeze-out stage, this phenomenon influences the r -process abundance pattern within the $A = 170 - 178$ region, primarily as a result of the β -decay processes that are accompanied by neutron emission. In addition, it is found that the neutron separation energies predicted by the pseudo DRHBc mass table show a non-monotonic behavior as A increases and represent a bump around $A = 175 - 182$. This leads to abundance ratios of adjacent even-even isotopes, as shown in Fig. 9(c), being less than 1 around $A = 172 - 176$ and larger than 1 for $A > 176$, thus forming a minimum near $A = 176$. Correspondingly, the relative abundances predicted by the pseudo DRHBc mass table exhibit a trough around $A = 176$, as shown in Fig. 9 (d). This simulated abundance trough, due to non-monotonic behavior of neutron separation energies, is also noted in Ref. [102]. The rapid shape transitions from a prolate configuration to an oblate one may explain this non-monotonic behavior. As shown in Fig. 9 (a), the quadrupole deformation β_2 for the neodymium isotopes shows a rapid shape transitions from prolate to oblate at $A = 175$, corresponding to the predicted non-monotonic neutron separation energy changes.

The abundance trough around $A = 170$ from classical r -process simulation with the pseudo DRHBc mass table is significant. As it is very different from the observed solar r -process abundances, here we provide two more remarks:

- (i) First, from the view of nuclear structure, the rapid shape transitions have led to the abundance trough around $A = 170$. Rapid shape transitions occur due to the shape-coexistence of prolate and oblate configurations for nuclei in this region. In this sense, incorporating the triaxial deformation effects or the shape-mixed beyond-mean-field effects could potentially resolve this abundance trough.
- (ii) Second, from the view of r -process simulation, the present simulations are performed using the classical r -process model with some approximations. The sudden neutron freeze-out approximation could lead to an unrealistic final abundance distribution. In the dynamical r -process studies, the competition between neutron capture and β -decay during the gradual neutron freeze-out stage can redistribute the abundance distribution and smooth local troughs to some extent. In this sense, this abundance trough could be partially eliminated in the full-network dynamical r -process simulations.
- (iii) Third, from the view of methodology, this abundance trough might only appear in the present pseudo DRHBc mass table. Although the pseudo DRHBc mass predictions

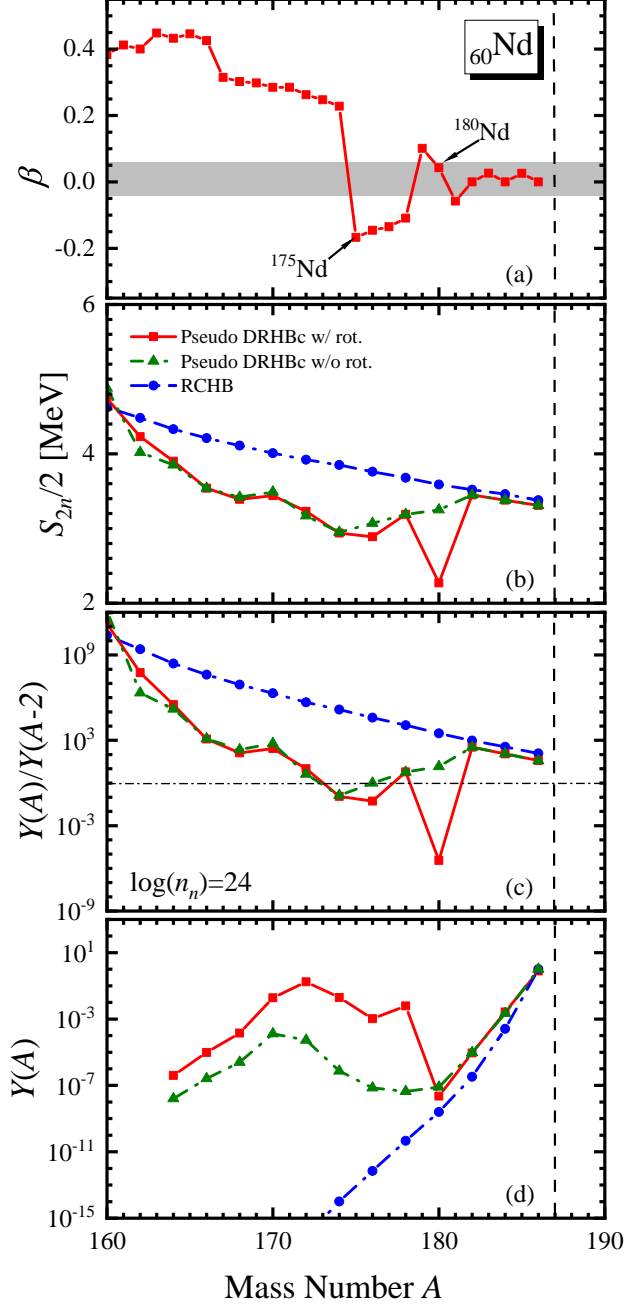


FIG. 9. (a) The nuclear quadrupole deformations β_2 of neodymium isotopes predicted by the DRHBc theory as a function of mass number A . (b) The neutron separation energies of the neodymium isotope chain predicted by the pseudo DRHBc and RCHB mass tables as functions of mass number A . (c) The abundance ratio of adjacent even-even nuclei along the neodymium isotope chain predicted by the pseudo DRHBc and RCHB mass tables as functions of mass number A , under astrophysical conditions with neutron number density $n_n = 10^{24} \text{ cm}^{-3}$ and temperature $T = 1.5 \text{ K}$. (d) Relative abundance distribution of even-even nuclei along the neodymium isotope chain predicted by the pseudo DRHBc and RCHB mass tables as functions of mass number A .

are very close to the real DRHBc results, the method of estimation employed in the present work is still not expected to be as effective as the real DRHBc calculations in dealing with the odd-even effects, which could lead to certain deviations in the results. One can expect the release of the full DRHBc mass table and test whether the abundance trough would appear.

V. SUMMARY

In summary, based on the available even- Z part of the DRHBc mass table, the masses of odd- Z nuclei are estimated by approximating the odd-even mass differences with average pairing gaps. A pseudo DRHBc mass table is constructed, and applied to r -process simulation.

The estimation is realized by expressing the mass of an odd nucleus as a function of its neighboring even ones' masses and odd-even mass differences, where the latter are approximated by the average pairing gaps. This treatment is examined by taking all even-odd nuclei with $8 \leq Z \leq 120$ as examples and estimating their binding energies based on the DRHBc results of even-even nuclei. It is found that the estimated binding energies of even-odd nuclei can effectively reproduce the self-consistent DRHBc calculation results. Then we estimate the binding energies of odd- Z nuclei based on the DRHBc results of even- Z nuclei, and combine them to construct a pseudo DRHBc mass table for all the nuclei with $8 \leq Z \leq 120$. The rms deviation of binding energy from available data $\sigma = 2.52$ MeV (without rotational correction) and 1.50 MeV (with rotational correction). The one/two-neutron/proton separation energies as well as their accuracies are also calculated and found to be close to the real DRHBc results from self-consistent calculations.

The r -process simulation is performed based on the obtained pseudo DRHBc mass table, and the impact of nuclear deformation effect is analyzed via comparing with results from the RCHB mass table. The simulations from both mass tables predict abundance peaks near $A = 130, 195$ and an abundance trough around $A = 170$. Compared to the RCHB mass table, the pseudo DRHBc mass table predicts higher abundances in $A = 148 - 165$ and lower abundances in $A = 170 - 180$. These differences can be explained by the r -process path nuclei predicted by the pseudo DRHBc mass tables; namely, around $A = 160$, they are closer to the stability line, while around $A = 175$ there is a gap. It is found that the differences

in the r -process path nuclei around $A = 160$ are caused by the faster decrease of neutron separation energies predicted by the pseudo DRHBc mass table along mass number A on the $Z = 54 - 58$ isotope chains. The absence of r -process path nuclei around $A = 175$ is attributed to the non-monotonic behavior of neutron separation energy and also influenced by the treatment of rotational corrections in the present DRHBc calculations. Detailed analysis indicates that both of these two differences originate from the deformation effects.

For perspective, full-network dynamical r -process simulations based on the upcoming full DRHBc mass table will be essential to clarify the abundance trough around $A = 170$. Incorporating the triaxial deformation and the beyond-mean-field effects in the DRHBc calculations for several key nuclei are also crucial, as more sufficient descriptions for nuclei with rapid shape transitions could be provided. Further improvements are expected based on these extensions.

ACKNOWLEDGMENTS

Helpful discussions with members of the DRHBc Mass Table Collaboration are highly appreciated. This work was partly supported by the National Natural Science Foundation of China under Grants No. 12405134, No. 12435006, No. 12141501, and No. 12475117, No. 11935003, the State Key Laboratory of Nuclear Physics and Technology, Peking University under Grants No. NPT2023KFY02, and No. NPT2023ZX03, the National Key Laboratory of Neutron Science and Technology under Grant No. NST202401016, National Key R&D Program of China 2024YFE0109803, High-performance Computing Platform of Peking University, the China Postdoctoral Science Foundation under Grant No. 2021M700256, and the start-up Grant No. XRC-23103 of Fuzhou University.

-
- [1] T. Yamaguchi, H. Koura, Y. Litvinov, and M. Wang, Masses of exotic nuclei, *Prog. Part. Nucl. Phys.* **120**, 103882 (2021).
 - [2] T. Kajino, W. Aoki, A. B. Balantekin, R. Diehl, M. A. Famiano, and G. J. Mathews, Current status of r -process nucleosynthesis, *Prog. Part. Nucl. Phys.* **107**, 109 (2019).
 - [3] A. de Roubin, D. Atanasov, K. Blaum, S. George, F. Herfurth, D. Kisler, M. Kowalska, S. Kreim, D. Lunney, V. Manea, E. Minaya Ramirez, M. Mougeot, D. Neidherr, M. Rosen-

- busch, L. Schweikhard, A. Welker, F. Wienholtz, R. N. Wolf, and K. Zuber, Nuclear deformation in the $A \approx 100$ region: Comparison between new masses and mean-field predictions, *Phys. Rev. C* **96**, 014310 (2017).
- [4] E. M. Ramirez, D. Ackermann, K. Blaum, M. Block, C. Droese, C. E. Düllmann, M. Dworschak, M. Eibach, S. Eliseev, E. Haettner, F. Herfurth, F. P. Heßberger, S. Hofmann, J. Ketelaer, G. Marx, M. Mazzocco, D. Nesterenko, Y. N. Novikov, W. R. Plaß, D. Rodríguez, C. Scheidenberger, L. Schweikhard, P. G. Thirolf, and C. Weber, Direct mapping of nuclear shell effects in the heaviest elements, *Science* **337**, 1207 (2012).
- [5] F. Wienholtz, D. Beck, K. Blaum, C. Borgmann, M. Breitenfeldt, R. B. Cakirli, S. George, F. Herfurth, J. D. Holt, M. Kowalska, S. Kreim, D. Lunney, V. Manea, J. Menéndez, D. Neidherr, M. Rosenbusch, L. Schweikhard, A. Schwenk, J. Simonis, J. Stanja, R. N. Wolf, and K. Zuber, Masses of exotic calcium isotopes pin down nuclear forces, *Nature* **498**, 346 (2013).
- [6] H. A. Bethe, Energy production in stars, *Phys. Rev.* **55**, 434 (1939).
- [7] M. R. Mumpower, R. Surman, D.-L. Fang, M. Beard, P. Möller, T. Kawano, and A. Aprahamian, Impact of individual nuclear masses on r -process abundances, *Phys. Rev. C* **92**, 035807 (2015).
- [8] M. Wang, W. J. Huang, F. G. Kondev, G. Audi, and S. Naimi, The AME 2020 atomic mass evaluation (II). tables, graphs and references, *Chin. Phys. C* **45**, 030003 (2021).
- [9] E. M. Burbidge, G. R. Burbidge, W. A. Fowler, and F. Hoyle, Synthesis of the elements in stars, *Rev. Mod. Phys.* **29**, 547 (1957).
- [10] F.-K. Thielemann, M. Eichler, I. Panov, and B. Wehmeyer, Neutron star mergers and nucleosynthesis of heavy elements, *Annu. Rev. Nucl. Part. Sci.* **67**, 253 (2017).
- [11] J. J. Cowan, C. Sneden, J. E. Lawler, A. Aprahamian, M. Wiescher, K. Langanke, G. Martínez-Pinedo, and F.-K. Thielemann, Origin of the heaviest elements: The rapid neutron-capture process, *Rev. Mod. Phys.* **93**, 015002 (2021).
- [12] B. Zhao and S. Q. Zhang, The r -process with the newly developed high-precision mass model WS4, *Astrophys. J.* **874**, 5 (2019).
- [13] A. Arcones and F.-K. Thielemann, Origin of the elements, *Astron. Astrophys. Rev.* **31**, 1 (2023).
- [14] X.-H. Wu and J. Meng, Supporting the cmb cosmic age from nuclear physics, *Sci. Bull.* **68**, 539 (2023).

- [15] M. R. Mumpower, R. Surman, G. C. McLaughlin, and A. Aprahamian, The impact of individual nuclear properties on r-process nucleosynthesis, *Prog. Part. Nucl. Phys.* **86**, 86 (2016).
- [16] X. H. Wu, P. W. Zhao, S. Q. Zhang, and J. Meng, High-precision nuclear chronometer for the cosmos, *Astrophys. J.* **941**, 152 (2022).
- [17] X. F. Jiang, X. H. Wu, and P. W. Zhao, Sensitivity study of r-process abundances to nuclear masses, *Astrophys. J.* **915**, 29 (2021).
- [18] J. Pearson, R. Nayak, and S. Goriely, Nuclear mass formula with bogolyubov-enhanced shell-quenching: application to r-process, *Phys. Lett. B* **387**, 455 (1996).
- [19] N. Wang, M. Liu, X. Wu, and J. Meng, Surface diffuseness correction in global mass formula, *Phys. Lett. B* **734**, 215 (2014).
- [20] P. Möller, A. J. Sierk, T. Ichikawa, and H. Sagawa, Nuclear ground-state masses and deformations: FRDM(2012), *At. Data Nucl. Data Tables* **109-110**, 1 (2016).
- [21] H. Koura, T. Tachibana, M. Uno, and M. Yamada, Nuclidic Mass Formula on a Spherical Basis with an Improved Even-Odd Term, *Prog. Theor. Phys.* **113**, 305 (2005).
- [22] S. Goriely, N. Chamel, and J. M. Pearson, Skyrme-hartree-fock-bogoliubov nuclear mass formulas: Crossing the 0.6 meV accuracy threshold with microscopically deduced pairing, *Phys. Rev. Lett.* **102**, 152503 (2009).
- [23] S. Goriely, S. Hilaire, M. Girod, and S. Péru, First gogny-hartree-fock-bogoliubov nuclear mass model, *Phys. Rev. Lett.* **102**, 242501 (2009).
- [24] D. Peña-Arteaga, S. Goriely, and N. Chamel, Relativistic mean-field mass models, *Eur. Phys. J. A* **52**, 320 (2016).
- [25] X. W. Xia, Y. Lim, P. W. Zhao, H. Z. Liang, X. Y. Qu, Y. Chen, H. Liu, L. F. Zhang, S. Q. Zhang, Y. Kim, and J. Meng, The limits of the nuclear landscape explored by the relativistic continuum Hartree-Bogoliubov theory, *At. Data Nucl. Data Tables* **121-122**, 1 (2018).
- [26] Y. L. Yang, Y. K. Wang, P. W. Zhao, and Z. P. Li, Nuclear landscape in a mapped collective Hamiltonian from covariant density functional theory, *Phys. Rev. C* **104**, 054312 (2021).
- [27] K. Zhang, M.-K. Cheoun, Y.-B. Choi, P. S. Chong, J. Dong, Z. Dong, X. Du, L. Geng, E. Ha, X.-T. He, C. Heo, M. C. Ho, E. J. In, S. Kim, Y. Kim, C.-H. Lee, J. Lee, H. Li, Z. Li, T. Luo, J. Meng, M.-H. Mun, Z. Niu, C. Pan, P. Papakonstantinou, X. Shang, C. Shen, G. Shen, W. Sun, X.-X. Sun, C. K. Tam, Thavayongnou, C. Wang, X. Wang, S. H. Wong, J. Wu, X. Wu, X. Xia, Y. Yan, R. W.-Y. Yeung, T. C. Yiu, S. Zhang, W. Zhang, X. Zhang, Q. Zhao,

- and S.-G. Zhou, Nuclear mass table in deformed relativistic Hartree-Bogoliubov theory in continuum, I: Even-even nuclei, *Atom. Data Nucl. Data Tabl.* **144**, 101488 (2022).
- [28] R. Utama, J. Piekarewicz, and H. B. Prosper, Nuclear mass predictions for the crustal composition of neutron stars: A bayesian neural network approach, *Phys. Rev. C* **93**, 014311 (2016).
- [29] L. Neufcourt, Y. C. Cao, W. Nazarewicz, and F. Viens, Bayesian approach to model-based extrapolation of nuclear observables, *Phys. Rev. C* **98**, 034318 (2018).
- [30] L. Neufcourt, Y. Cao, W. Nazarewicz, E. Olsen, and F. Viens, Neutron drip line in the ca region from bayesian model averaging, *Phys. Rev. Lett.* **122**, 062502 (2019).
- [31] X. H. Wu and P. W. Zhao, Predicting nuclear masses with the kernel ridge regression, *Phys. Rev. C* **101**, 051301 (2020).
- [32] X. H. Wu, L. H. Guo, and P. W. Zhao, Nuclear masses in extended kernel ridge regression with odd-even effects, *Phys. Lett. B* **819**, 136387 (2021).
- [33] Z. M. Niu and H. Z. Liang, Nuclear mass predictions with machine learning reaching the accuracy required by r -process studies, *Phys. Rev. C* **106**, L021303 (2022).
- [34] X.-K. Du, P. Guo, X.-H. Wu, and S.-Q. Zhang, Examination of machine learning for assessing physical effects: Learning the relativistic continuum mass table with kernel ridge regression*, *Chin. Phys. C* **47**, 074108 (2023).
- [35] X. H. Wu, C. Pan, K. Y. Zhang, and J. Hu, Nuclear mass predictions of the relativistic continuum hartree-bogoliubov theory with the kernel ridge regression, *Phys. Rev. C* **109**, 024310 (2024).
- [36] X. H. Wu and C. Pan, Nuclear mass predictions with anisotropic kernel ridge regression, *Phys. Rev. C* **110**, 034322 (2024).
- [37] X. H. Wu and P. W. Zhao, Principal components of nuclear mass models, *Sci. China-Phys. Mech. Astron.* **67**, 272011 (2024).
- [38] Y. Y. Guo, T. Yu, X. H. Wu, C. Pan, and K. Y. Zhang, Nuclear mass predictions of the relativistic continuum hartree-bogoliubov theory with the kernel ridge regression. ii. odd-even effects, *Phys. Rev. C* **110**, 064310 (2024).
- [39] P. W. Zhao, L. S. Song, B. Sun, H. Geissel, and J. Meng, Crucial test for covariant density functional theory with new and accurate mass measurements from Sn to Pa, *Phys. Rev. C* **86**, 064324 (2012).

- [40] K. Zhang, X. He, J. Meng, C. Pan, C. Shen, C. Wang, and S. Zhang, Predictive power for superheavy nuclear mass and possible stability beyond the neutron drip line in deformed relativistic Hartree-Bogoliubov theory in continuum, *Phys. Rev. C* **104**, L021301 (2021).
- [41] X.-T. He, J.-W. Wu, K.-Y. Zhang, and C.-W. Shen, Odd-even differences in the stability “peninsula” in the $106 \leq Z \leq 112$ region with the deformed relativistic Hartree-Bogoliubov theory in continuum, *Phys. Rev. C* **110**, 014301 (2024).
- [42] J. Meng, H. Toki, S. G. Zhou, S. Q. Zhang, W. H. Long, and L. S. Geng, Relativistic continuum Hartree Bogoliubov theory for ground-state properties of exotic nuclei, *Prog. Part. Nucl. Phys.* **57**, 470 (2006).
- [43] J. Dobaczewski, H. Flocard, and J. Treiner, Hartree-Fock-Bogolyubov description of nuclei near the neutron-drip line, *Nucl. Phys. A* **422**, 103 (1984).
- [44] J. Dobaczewski, W. Nazarewicz, T. R. Werner, J. F. Berger, C. R. Chinn, and J. Dechargé, Mean-field description of ground-state properties of drip-line nuclei: Pairing and continuum effects, *Phys. Rev. C* **53**, 2809 (1996).
- [45] M. Grasso, N. Sandulescu, N. Van Giai, and R. J. Liotta, Pairing and continuum effects in nuclei close to the drip line, *Phys. Rev. C* **64**, 064321 (2001).
- [46] N. Michel, K. Matsuyanagi, and M. Stoitsov, Gamow-hartree-fock-bogoliubov method: Representation of quasiparticles with berggren sets of wave functions, *Phys. Rev. C* **78**, 044319 (2008).
- [47] J. C. Pei, A. T. Kruppa, and W. Nazarewicz, Quasiparticle continuum and resonances in the hartree-fock-bogoliubov theory, *Phys. Rev. C* **84**, 024311 (2011).
- [48] Y. N. Zhang, J. C. Pei, and F. R. Xu, Hartree-Fock-Bogoliubov descriptions of deformed weakly bound nuclei in large coordinate spaces, *Phys. Rev. C* **88**, 054305 (2013).
- [49] J. Meng and P. Ring, Relativistic Hartree-Bogoliubov Description of the Neutron Halo in ^{11}Li , *Phys. Rev. Lett.* **77**, 3963 (1996).
- [50] J. Meng, Relativistic continuum Hartree-Bogoliubov theory with both zero range and finite range Gogny force and their application, *Nucl. Phys. A* **635**, 3 (1998).
- [51] J. Meng and P. Ring, Giant Halo at the Neutron Drip Line, *Phys. Rev. Lett.* **80**, 460 (1998).
- [52] S.-G. Zhou, J. Meng, P. Ring, and E.-G. Zhao, Neutron halo in deformed nuclei, *Phys. Rev. C* **82**, 011301 (2010).
- [53] L. Li, J. Meng, P. Ring, E.-G. Zhao, and S.-G. Zhou, Deformed relativistic Hartree-

- Bogoliubov theory in continuum, Phys. Rev. C **85**, 024312 (2012).
- [54] X.-X. Sun, J. Zhao, and S.-G. Zhou, Shrunk halo and quenched shell gap at $N = 16$ in ^{22}C : Inversion of sd states and deformation effects, Phys. Lett. B **785**, 530 (2018).
- [55] K. Y. Zhang, D. Y. Wang, and S. Q. Zhang, Effects of pairing, continuum, and deformation on particles in the classically forbidden regions for Mg isotopes, Phys. Rev. C **100**, 034312 (2019).
- [56] X.-X. Sun, J. Zhao, and S.-G. Zhou, Study of ground state properties of carbon isotopes with deformed relativistic Hartree-Bogoliubov theory in continuum, Nucl. Phys. A **1003**, 122011 (2020).
- [57] Z. H. Yang, Y. Kubota, A. Corsi, K. Yoshida, X.-X. Sun, J. G. Li, M. Kimura, N. Michel, K. Ogata, C. X. Yuan, Q. Yuan, G. Authelet, H. Baba, C. Caesar, D. Calvet, A. Delbart, M. Dozono, J. Feng, F. Flavigny, J.-M. Gheller, J. Gibelin, A. Giganon, A. Gillibert, K. Hasegawa, T. Isobe, Y. Kanaya, S. Kawakami, D. Kim, Y. Kiyokawa, M. Kobayashi, N. Kobayashi, T. Kobayashi, Y. Kondo, Z. Korkulu, S. Koyama, V. Lapoux, Y. Maeda, F. M. Marqués, T. Motobayashi, T. Miyazaki, T. Nakamura, N. Nakatsuka, Y. Nishio, A. Obertelli, A. Ohkura, N. A. Orr, S. Ota, H. Otsu, T. Ozaki, V. Panin, S. Paschalis, E. C. Pollacco, S. Reichert, J.-Y. Roussé, A. T. Saito, S. Sakaguchi, M. Sako, C. Santamaria, M. Sasano, H. Sato, M. Shikata, Y. Shimizu, Y. Shindo, L. Stuhl, T. Sumikama, Y. L. Sun, M. Tabata, Y. Togano, J. Tsubota, F. R. Xu, J. Yasuda, K. Yoneda, J. Zenihiro, S.-G. Zhou, W. Zuo, and T. Uesaka, Quasifree neutron knockout reaction reveals a small s -orbital component in the borromean nucleus ^{17}B , Phys. Rev. Lett. **126**, 082501 (2021).
- [58] X.-X. Sun, Deformed two-neutron halo in ^{19}B , Phys. Rev. C **103**, 054315 (2021).
- [59] S.-Y. Zhong, S.-S. Zhang, X.-X. Sun, and M. S. Smith, Study of the deformed halo nucleus ^{31}Ne with Glauber model based on microscopic self-consistent structures, Sci. China Phys. Mech. Astron. **65**, 262011 (2022).
- [60] K. Y. Zhang, P. Papakonstantinou, M.-H. Mun, Y. Kim, H. Yan, and X.-X. Sun, Collapse of the $N = 28$ shell closure in the newly discovered ^{39}Na nucleus and the development of deformed halos towards the neutron dripline, Phys. Rev. C **107**, L041303 (2023).
- [61] K. Y. Zhang, S. Q. Yang, J. L. An, S. S. Zhang, P. Papakonstantinou, M.-H. Mun, Y. Kim, and H. Yan, Missed prediction of the neutron halo in ^{37}Mg , Phys. Lett. B **844**, 138112 (2023).
- [62] J.-L. An, K.-Y. Zhang, Q. Lu, S.-Y. Zhong, and S.-S. Zhang, A unified description of the

- halo nucleus ^{37}Mg from microscopic structure to reaction observables, *Phys. Lett. B* **849**, 138422 (2024).
- [63] C. Pan, K. Zhang, and S. Zhang, Nuclear magnetism in the deformed halo nucleus ^{31}Ne , *Phys. Lett. B* **855**, 138792 (2024).
- [64] K. Y. Zhang, C. Pan, and S. Wang, Examination of the evidence for a proton halo in ^{22}Al , *Phys. Rev. C* **110**, 014320 (2024).
- [65] L.-Y. Wang, K. Zhang, J.-L. An, and S.-S. Zhang, Toward a unified description of the one-neutron halo nuclei ^{15}C and ^{19}C from structure to reaction, *Eur. Phys. J. A* **60**, 251 (2024).
- [66] C. Pan, K. Y. Zhang, P. S. Chong, C. Heo, M. C. Ho, J. Lee, Z. P. Li, W. Sun, C. K. Tam, S. H. Wong, R. W.-Y. Yeung, T. C. Yiu, and S. Q. Zhang, Possible bound nuclei beyond the two-neutron drip line in the $50 \leq z \leq 70$ region, *Phys. Rev. C* **104**, 024331 (2021).
- [67] X. He, C. Wang, K. Zhang, and C. Shen, Possible existence of bound nuclei beyond neutron drip lines driven by deformation, *Chin. Phys. C* **45**, 101001 (2021).
- [68] Y.-B. Choi, C.-H. Lee, M.-H. Mun, and Y. Kim, Bubble nuclei with shape coexistence in even-even isotopes of Hf to Hg, *Phys. Rev. C* **105**, 024306 (2022).
- [69] S. Kim, M.-H. Mun, M.-K. Cheoun, and E. Ha, Shape coexistence and neutron skin thickness of Pb isotopes by the deformed relativistic Hartree-Bogoliubov theory in continuum, *Phys. Rev. C* **105**, 034340 (2022).
- [70] M.-H. Mun, S. Kim, M.-K. Cheoun, W. Y. So, S. Choi, and E. Ha, Odd-even shape staggering and kink structure of charge radii of Hg isotopes by the deformed relativistic Hartree-Bogoliubov theory in continuum, *Phys. Lett. B* **847**, 138298 (2023).
- [71] P. Guo, C. Pan, Y. C. Zhao, X. K. Du, and S. Q. Zhang, Prolate-shape dominance in atomic nuclei within the deformed relativistic Hartree-Bogoliubov theory in continuum, *Phys. Rev. C* **108**, 014319 (2023).
- [72] Y. Xiao, S.-Z. Xu, R.-Y. Zheng, X.-X. Sun, L.-S. Geng, and S.-S. Zhang, One-proton emission from $^{148-151}\text{Lu}$ in the DRHBc+WKB approach, *Phys. Lett. B* **845**, 138160 (2023).
- [73] Y.-B. Choi, C.-H. Lee, M.-H. Mun, S. Choi, and Y. Kim, α -decay half-lives for even-even isotopes of w to u, *Phys. Rev. C* **109**, 054310 (2024).
- [74] Q. Lu, K.-Y. Zhang, and S.-S. Zhang, Triaxial shape of the one-proton emitter ^{149}Lu , *Phys. Lett. B* **856**, 138922 (2024).
- [75] K. Zhang, M.-K. Cheoun, Y.-B. Choi, P. S. Chong, J. Dong, L. Geng, E. Ha, X. He, C. Heo,

- M. C. Ho, E. J. In, S. Kim, Y. Kim, C.-H. Lee, J. Lee, Z. Li, T. Luo, J. Meng, M.-H. Mun, Z. Niu, C. Pan, P. Papakonstantinou, X. Shang, C. Shen, G. Shen, W. Sun, X.-X. Sun, C. K. Tam, Thavayongnou, C. Wang, S. H. Wong, X. Xia, Y. Yan, R. W.-Y. Yeung, T. C. Yiu, S. Zhang, W. Zhang, and S.-G. Zhou (DRHBc Mass Table Collaboration), Deformed relativistic Hartree-Bogoliubov theory in continuum with a point-coupling functional: Examples of even-even Nd isotopes, *Phys. Rev. C* **102**, 024314 (2020).
- [76] C. Pan, M.-K. Cheoun, Y.-B. Choi, J. Dong, X. Du, X.-H. Fan, W. Gao, L. Geng, E. Ha, X.-T. He, J. Huang, K. Huang, S. Kim, Y. Kim, C.-H. Lee, J. Lee, Z. Li, Z.-R. Liu, Y. Ma, J. Meng, M.-H. Mun, Z. Niu, P. Papakonstantinou, X. Shang, C. Shen, G. Shen, W. Sun, X.-X. Sun, J. Wu, X. Wu, X. Xia, Y. Yan, T. C. Yiu, K. Zhang, S. Zhang, W. Zhang, X. Zhang, Q. Zhao, R. Zheng, and S.-G. Zhou (DRHBc Mass Table Collaboration), Deformed relativistic Hartree-Bogoliubov theory in continuum with a point-coupling functional. II. examples of odd Nd isotopes, *Phys. Rev. C* **106**, 014316 (2022).
- [77] P. Guo, X. Cao, K. Chen, Z. Chen, M.-K. Cheoun, Y.-B. Choi, P. C. Lam, W. Deng, J. Dong, P. Du, X. Du, K. Duan, X. Fan, W. Gao, L. Geng, E. Ha, X.-T. He, J. Hu, J. Huang, K. Huang, Y. Huang, Z. Huang, K. D. Hyung, H. Y. Chan, X. Jiang, S. Kim, Y. Kim, C.-H. Lee, J. Lee, J. Li, M. Li, Z. Li, Z. Li, Z. Lian, H. Liang, L. Liu, X. Lu, Z.-R. Liu, J. Meng, Z. Meng, M.-H. Mun, Y. Niu, Z. Niu, C. Pan, J. Peng, X. Qu, P. Papakonstantinou, T. Shang, X. Shang, C. Shen, G. Shen, T. Sun, X.-X. Sun, S. Wang, T. Wang, Y. Wang, Y. Wang, J. Wu, L. Wu, X. Wu, X. Xia, H. Xie, J. Yao, K. Y. Ip, T. C. Yiu, J. Yu, Y. Yu, K. Zhang, S. Zhang, S. Zhang, W. Zhang, X. Zhang, Y. Zhang, Y. Zhang, Y. Zhang, Z. Zhang, Q. Zhao, Y. Zhao, R. Zheng, C. Zhou, S.-G. Zhou, and L. Zou, Nuclear mass table in deformed relativistic Hartree-Bogoliubov theory in continuum, II: Even- Z nuclei, *Atomic Data and Nuclear Data Tables* **158**, 101661 (2024).
- [78] H. Kucharek and P. Ring, Relativistic field theory of superfluidity in nuclei, *Z. Phys. A* **339**, 23 (1991).
- [79] P. Ring and P. Schuck, *The Nuclear Many-Body Problem* (Springer-Verlag, 1980).
- [80] S.-G. Zhou, J. Meng, and P. Ring, Spherical relativistic Hartree theory in a Woods-Saxon basis, *Phys. Rev. C* **68**, 034323 (2003).
- [81] K. Y. Zhang, C. Pan, and S. Q. Zhang, Optimized Dirac Woods-Saxon basis for covariant density functional theory, *Phys. Rev. C* **106**, 024302 (2022).

- [82] L.-L. Li, J. Meng, P. Ring, E.-G. Zhao, and S.-G. Zhou, Odd Systems in Deformed Relativistic Hartree Bogoliubov Theory in Continuum, *Chin. Phys. Lett.* **29**, 042101 (2012).
- [83] S. E. Agbemava, A. V. Afanasjev, D. Ray, and P. Ring, Global performance of covariant energy density functionals: Ground state observables of even-even nuclei and the estimate of theoretical uncertainties, *Phys. Rev. C* **89**, 054320 (2014).
- [84] A. V. Afanasjev, S. E. Agbemava, D. Ray, and P. Ring, Neutron drip line: Single-particle degrees of freedom and pairing properties as sources of theoretical uncertainties, *Phys. Rev. C* **91**, 014324 (2015).
- [85] K.-L. Kratz, J.-P. Bitouzet, F.-K. Thielemann, P. Moeller, and B. Pfeiffer, Isotopic *r*-Process Abundances and Nuclear Structure Far from Stability: Implications for the *r*-Process Mechanism, *Astrophys. J.* **403**, 216 (1993).
- [86] K.-L. Kratz, K. Farouqi, B. Pfeiffer, J. W. Truran, C. Sneden, and J. J. Cowan, Explorations of the *r*-Processes: Comparisons between Calculations and Observations of Low-Metallicity Stars, *Astrophys. J.* **662**, 39 (2007).
- [87] B. Sun, F. Montes, L. S. Geng, H. Geissel, Y. A. Litvinov, and J. Meng, Application of the relativistic mean-field mass model to the *r*-process and the influence of mass uncertainties, *Phys. Rev. C* **78**, 025806 (2008).
- [88] X. D. Xu, B. Sun, Z. M. Niu, Z. Li, Y.-Z. Qian, and J. Meng, Reexamining the temperature and neutron density conditions for *r*-process nucleosynthesis with augmented nuclear mass models, *Phys. Rev. C* **87**, 015805 (2013).
- [89] B. Chen, J. Dobaczewski, K.-L. Kratz, K. Langanke, B. Pfeiffer, F.-K. Thielemann, and P. Vogel, Influence of shell-quenching far from stability on the astrophysical *r*-process, *Phys. Lett. B* **355**, 37 (1995).
- [90] J. J. Cowan, F.-K. Thielemann, and J. W. Truran, The *r*-process and nucleochronology, *Phys. Rep.* **208**, 267 (1991).
- [91] Y.-Z. Qian, The origin of the heavy elements: Recent progress in the understanding of the *r*-process, *Prog. Part. Nucl. Phys.* **50**, 153 (2003).
- [92] M. Arnould, S. Goriely, and K. Takahashi, The *r*-process of stellar nucleosynthesis: Astrophysics and nucl. phys. achievements and mysteries, *Phys. Rep.* **450**, 97 (2007).
- [93] M. Kortelainen, T. Lesinski, J. Moré, W. Nazarewicz, J. Sarich, N. Schunck, M. V. Stoitsov, and S. Wild, Nuclear energy density optimization, *Phys. Rev. C* **82**, 024313 (2010).

- [94] E. Olsen, M. Pfützner, N. Birge, M. Brown, W. Nazarewicz, and A. Perhac, Landscape of two-proton radioactivity, *Phys. Rev. Lett.* **110**, 222501 (2013).
- [95] J. Dobaczewski, W. Nazarewicz, and T. R. Werner, Closed shells at drip-line nuclei, *Phys. Scr.* **1995**, 15 (1995).
- [96] T. Duguet, P. Bonche, P.-H. Heenen, and J. Meyer, Pairing correlations. I. Description of odd nuclei in mean-field theories, *Phys. Rev. C* **65**, 014310 (2001).
- [97] T. Duguet, P. Bonche, P.-H. Heenen, and J. Meyer, Pairing correlations. II. Microscopic analysis of odd-even mass staggering in nuclei, *Phys. Rev. C* **65**, 014311 (2001).
- [98] P. W. Zhao, Z. P. Li, J. M. Yao, and J. Meng, New parametrization for the nuclear covariant energy density functional with a point-coupling interaction, *Phys. Rev. C* **82**, 054319 (2010).
- [99] Z. Yong, L. Zhihong, C. Yongshou, W. Youbao, S. Jun, G. Bing, and L. Weiping, Estimate of β -decay half-lives for r-process nuclei, *Nucl. Phys. Rev.* **34**, 425 (2017).
- [100] G. Audi, A. Wapstra, and C. Thibault, The ame2003 atomic mass evaluation: (II). tables, graphs and references, *Nucl. Phys. A* **729**, 337 (2003).
- [101] C. Sneden, J. J. Cowan, and R. Gallino, Neutron-capture elements in the early galaxy, *Annu. Rev. Nucl. Part. Sci.* **46**, 241 (2008).
- [102] D. Martin, A. Arcones, W. Nazarewicz, and E. Olsen, Impact of nuclear mass uncertainties on the r process, *Phys. Rev. Lett.* **116**, 121101 (2016).